Relaxometry Studies of a Highly Stable Nanoscale Metal–Organic Framework Made of Cu(II), Gd(III), and the Macrocyclic DOTP

Arnau Carné-Sánchez,[†] Célia S. Bonnet,[‡] Inhar Imaz,[†] Julia Lorenzo,[§] Éva Tóth,*[‡] and Daniel Maspoch*[†,⊥]

[†]Institut Catala de Nanociencia i Nanotecnologia, Esfera UAB, 08193 Bellaterra, Spain
[‡]Centre de Biophysique Moléculaire, CNRS, Rue Charles Sadron, 45071 Orléans, France
[§]Institut de Biotecnologia i Biomedicina, UAB, 08193 Bellaterra, Spain
[⊥]Institució Catalana de Recerca i Estudis Avançats, 08100 Barcelona, Spain

S *Supporting Information*

ABSTRACT: The macrocyclic ligand DOTP is used to assemble a porous, heterometallic metal–organic framework (MOF). This MOF is miniaturizable down to the nanoscale to form stable colloids, is stable in physiological saline solution and cell culture media, and is not cytotoxic. It shows interesting relaxometric properties with r_1 at high field (500 MHz) of 5 mM^{-1}·s^{-1} and a maximum r_1 = 15 mM^{-1}·s^{-1} at 40 MHz, which remains constant over a wide pH range and increases with temperature.

Magnetic resonance imaging (MRI) is one of the most powerful diagnostic tools in medical science thanks to its noninvasive character and sub-millimeter spatial resolution. Based on the detection of nuclear spin reorientations under a magnetic field, MRI has been demonstrated to be very effective for assessing anatomical changes and monitoring organ functions. However, in many cases, the use of contrast agents (CAs) is necessary to enhance the intrinsic contrast of MR images; 35% of clinical MRI scans are currently performed with the assistance of CAs.[1] These paramagnetic or superparamagnetic substances act by shortening proton longitudinal (T1) and/or transverse (T2) relaxation times of water protons, improving the contrast between diseased and normal tissue. Most of the currently used CAs are stable chelates of the highly paramagnetic Gd(III) ion;[2] however, some limitations persist due to their low sensitivity, lack of selectivity, and low retention time that make them effective only in areas of high accumulation. Nanoparticulate Gd(III)-based CAs can provide increased *in vivo* circulation time and slower rotational tumbling of the agent and contain a high payload of Gd(III) ions per particle, giving rise to superior MRI efficacies.[3] The most common approaches for developing such nanoscale CAs involve the use of Gd(III) oxide nanoparticles[4] and the introduction of Gd(III) chelates in a variety of nanotemplates, such as inorganic nanoparticles,[5] dendrimers,[6] viral capsids,[7] proteins,[8] mesoporous silica,[9] colloidal self-assembled nanoparticles,[10] and zeolites.[11]
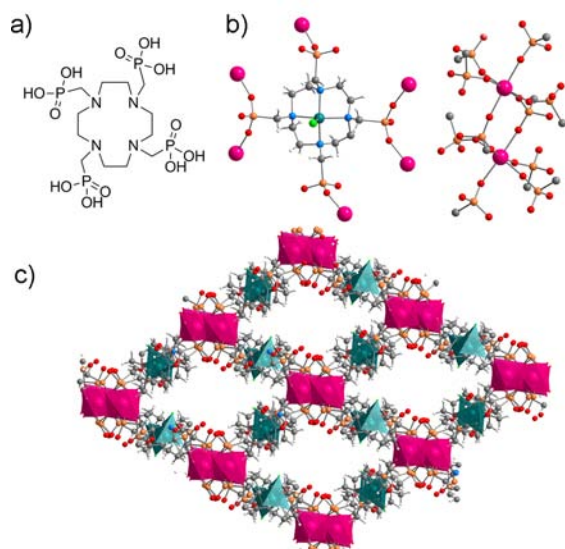
Nanoscale metal–organic frameworks (nanoMOFs),[12] which have the advantage of high surface areas and endless possibilities to carry high Gd(III) concentrations per nanocrystal unit, are beginning to be investigated as an alternative class of nanoscale CAs.[13] Primary examples are nanoMOFs assembled from Gd(III) ions and polycarboxylate linkers.[13−15] The biologically viable conception of CAs based on nanoMOFs remains, however, quite challenging. For example, MOFs typically lack stability in water and in body fluids, causing the release of highly toxic free Gd(III) ions and preventing detailed relaxometry studies. This stability is a critical issue toward the potential *in vivo* exploitation of CAs based on MOFs.

Herein we propose to construct a nanoMOF containing Gd(III) by using a macrocyclic ligand with multiple coordination sites in order to limit free Gd(III) leaching. In addition, we present for the first time a temperature- and pH-dependent, variable-field relaxometric study for a nanoMOF to gain insight into the mechanisms that govern the relaxation behavior of these compounds. The Gd(III)-based nanoMOF we have designed features high stability in physiological saline solution and in cell culture media, while it retains an interesting r_1 relaxivity of 15 mM^{-1}·s^{-1} at 40 MHz (25 °C) and r_1 = 5 mM^{-1}·s^{-1} at a higher field (500 MHz, 25 °C). Our concept relies on using the macrocyclic 1,4,7,10-tetraazacyclododecane-1,4,7,10-tetramethylenephosphonic acid (DOTP, Figure 1a) to assemble Gd(III) and Cu(II) ions to form a MOF structure with formula [GdCu(DOTP)Cl]·4.5H$_2$O (hereafter called **CAMOF-1**). Cu(II) is chelated inside the cage formed by DOTP, whereas Gd(III) is coordinated by phosphonate groups from different DOTP units, resulting in a porous three-dimensional structure. The choice of DOTP as the organic linker was governed by the following considerations: (1) it belongs to the family of strong chelating ligands capable of forming highly stable complexes with a variety of ligands;[16] (2) it offers a large number of metal binding sites of two distinct types of chemical nature, one at the phosphonate pendant arms and the other within the cyclen ring; (3) phosphonates form stronger bonds than carboxylates do with metal ions,[17] so its four phosphonate groups can be used to form highly stable MOFs in aqueous conditions; and (4) its strong chelating capabilities can be used to sequester the metal ions eventually released upon MOF decomposition, thus further helping to maintain low levels of leached free Gd(III) and Cu(II) ions. Cu(II) ions are also key actors in the formation of the MOF
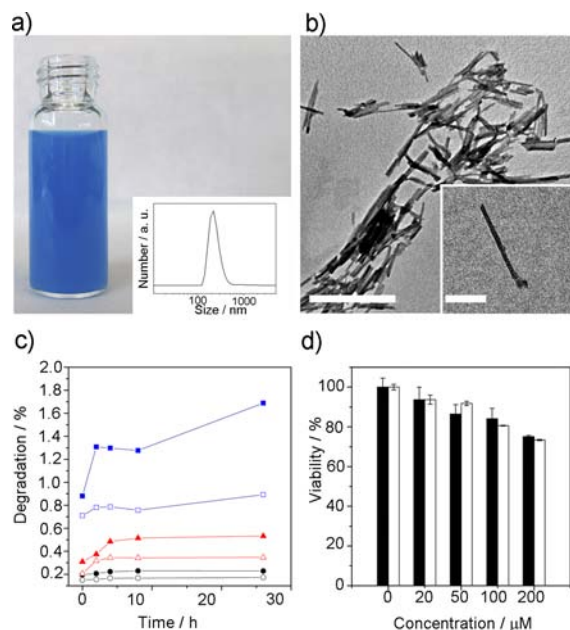
Figure 1. (a) Representation of DOTP ligand. (b) Crystal structure of **CAMOF-1**, showing the coordination of DOTP with one Cu(II) ion and six Gd(III) ions and the coordination geometry of Gd(III) ions. (c) 3D extended structure of **CAMOF-1**, showing the presence of 1D channels. Color code: Gd, pink; C, gray; N, blue; Cu, dark green; Cl, light green; O, red.

structure made of Gd(III) and DOTP: an extended structure is not formed when other secondary metal ions such as Zn(II), Ni(II), Co(II), Mn(II), Fe(III), and Mg(II) are used (Figure S2), likely because they have less preference for nitrogen donors with respect to Cu(II). Gd(III) and Cu(II) are the only ones that have comparably high stability constants with DOTP (28.8^{18} and $25.4,^{19}$ respectively). We hypothesize that this similarity makes it possible to disrupt the formation of the very stable mononuclear $[Gd(DOTP)]^{5-}$ species, allowing DOTP to simultaneously coordinate to the two different metal ions and extend the metal−organic structure. In addition to the preference of Cu(II) for nitrogen donors and the preference of lanthanides for oxygen donors, formation kinetic factors might also contribute to yield a structure in which the Cu(II) is in the polyamine cage and the Gd(III) is coordinated by the phosphonates. We discovered that the formation of **CAMOF-1** takes place over a wide pH range (pH = 3−8), and that the crystal size is affected by pH and temperature. Macrocrystals of **CAMOF-1**, suitable for single-crystal X-ray diffraction, have been assembled at low pHs (<4) and at high temperatures, whereas nanocrystals of **CAMOF-1** (hereafter called **nano-CAMOF-1**) have been prepared at high pHs (>6) and at room temperature.

In an initial experiment, macroscopic blue rod-like crystals of **CAMOF-1** were prepared upon reaction of $Gd(NO_3)_3\cdot6H_2O$, $CuCl_2$, and DOTP in water at 85 °C for 12 h. Here, square-pyramidal Cu(II) ions are coordinated to the four ring-nitrogen atoms defining the equatorial plane, whereas the axial position is occupied by a chlorine atom. The four deprotonated phosphonate groups of each DOTP are then coordinated to six octahedral Gd(III) ions, which are connected to six DOTP linkers via their phosphonate groups (Figure 1b) to form an extended three-dimensional porous framework with one-dimensional channels (~5 × 5 Å; 23% of void space in unit cell)[20] along the $(\bar{1}1\bar{3})$ direction (Figure 1c). Microporosity of **CAMOF-1** was confirmed by CO_2 gas adsorption studies at

195 K. It showed hysteretic behavior and a BET surface area of 110 $m^2\cdot g^{-1}$ (Figure S3).

In order to potentially use **CAMOF-1** as a CA, a requirement is to control its crystal size down to the nanometer length scale. This miniaturization step was done by reproducing the above-mentioned reaction at higher pHs. Subsequent addition of $CuCl_2$ and $Gd(NO_3)_3\cdot6H_2O$ to a partially deprotonated form of DOTP in water (pH = 8) at room temperature led to the formation of a very stable blue colloid of **nanoCAMOF-1** (Figure 2a). Transmission electron microscopy (TEM) images

Figure 2. (a) Photograph of **nanoCAMOF-1** colloidal suspension and its size distribution determined by DLS (inset). (b) TEM images of **nanoCAMOF-1**. Scale bars: 500 and 100 nm (inset). (c) Time dependence of the percentage of the total Gd(III) [filled symbols] and the maximum potential free Gd(III) [empty symbols] ions relative to the total Gd(III) content in **nanoCAMOF-1** leached upon incubation in saline solution at pH = 4 (black circles), 7.4 (red triangles), and 9 (blue squares) and at 37.5 °C. (d) Effects of **nanoCAMOF-1** on the viability of HepG2 (filled bars) and MCF7 (empty bars) cells at 24 h. Error bars represent the standard error.
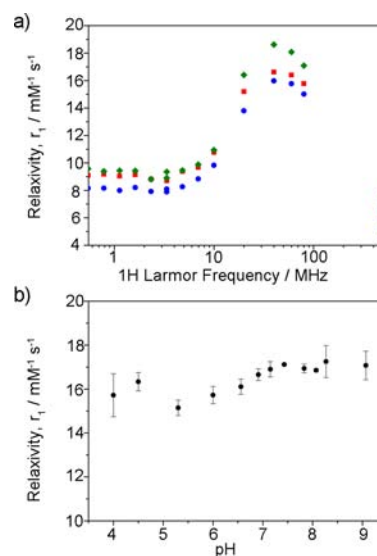
of the colloid demonstrated the formation of uniform nanowires 10 nm in diameter and 200 nm in length (Figure 2b). The average length of these nanowires was further confirmed by dynamic light scattering (DLS) measurements (Figure 2a, inset). Importantly, we were able to control the length of the nanowires by synthesizing them through a diffusion method: we obtained larger nanofibers (up to 100 μm) by diffusing an aqueous solution of $Gd(NO_3)_3\cdot6H_2O$ on an aqueous solution of $CuCl_2$ and DOTP (Figure S6). The correspondence between these nanostructures and **CAMOF-1** was confirmed by the positive matching between the elemental analyses, IR spectra, XRPD, and magnetic properties performed on these samples (Figure S5).

The strong Gd(III)−phosphonate bonds and the high connectivity of **nanoCAMOF-1** give it high stability in physiological saline solution (NaCl, 0.9% w/w) and in 4-(2-hydroxyethyl)-1-piperazineethanesulfonic acid (HEPES)-buffered media. To perform these experiments, as-synthesized (200 nm in length) **nanoCAMOF-1** was first centrifuged and redispersed in water three times, and finally redispersed in the

studied medium to form a stable colloid, as confirmed by DLS. Exposure of this material to saline solution at pH = 4, 7.4, and 9 and at T = 37.5 °C for 24 h led to the leaching of 0.2%, 0.5%, and 1.6% of the total Gd(III) and 0.2%, 0.4%, and 3.5% of the total Cu(II) content in **nanoCAMOF-1**, respectively, as determined by ICP-OES (Figures 2c and S7a). The maximum concentration of free Gd(III) ions in the incubated samples was also determined by titration with xylenol orange.[21] This study confirmed low maximum concentrations of free Gd(III) ions at all pHs, being 0.2% (11 μM), 0.4% (20 μM), and 0.9% (50 μM) of the total Gd(III) content in **nanoCAMOF-1** at pH = 4, 7.4, and 9, respectively. When exposed to HEPES buffer at pH = 7.4, **nanoCAMOF-1** leached 1.7% of the total Gd(III) and 1.4% of the total Cu(II) content in 24 h (Figure S7b). Further exposure of this material to these media for 1 week did not show a significant increase of leached Gd(III) and Cu(II) ions. In all cases, TEM and DLS analysis after 1 week of exposure confirmed no degradation of **nanoCAMOF-1** (Figures S8 and S9).

It is also important to note here that those differences between total leached Gd(III) and free leached Gd(III) in physiological saline solution at pH = 7.4 and 9 should be attributed to the capacity of DOTP to coordinate metal ions after partial degradation of the MOF. This was confirmed by mass spectrometry analysis of the leached products of the incubated samples. Analysis of the supernatants resulting from the degradation experiments using ESI-MS reveals species corresponding to CuDOTP and CuDOTPGd complexes ($[CuDOTP - 4H + 3Na]^+$ = 675.96, $[CuDOTP - 5H + 4Na]^+$ = 697.94, $[CuGdDOTP - 5H - OH]^+$ + 2MeOH = 810.96, $[CuGdDOTP - 5H - OH]^+$ + 2MeOH + H_2O = 828.92, $[CuGdDOTP - 6H - OH + Na]^+$ + 2MeOH = 832.96; Figures S10 and S11), establishing that certain percentages of Gd(III) and Cu(II) ions are indeed attached to DOTP in solution. These results are in agreement with the cytotoxicity assays conducted with two cell lines, HepG2 and MCF7. After 24 h of incubation, both cells showed good viability (75% for HepG2 and 74% for MCF7) up to 200 μM **nanoCAMOF-1** (Figure 2d). These results demonstrate that **nanoCAMOF-1** does not show significant toxicity resulting from the leakage of free toxic Gd(III) and Cu(II) ions. This lack of noticeable toxicity could be attributed to the capacity of DOTP to chelate a high percentage of the limited quantity of Gd(III) and Cu(II) ions leached upon degradation of **nanoCAMOF-1**.

The efficacy of **nanoCAMOF-1** as a potential CA for MRI was investigated by ^{1}H nuclear magnetic relaxation dispersion (i.e., NMRD relaxometry) profiles in the frequency range 10 kHz $\leq \nu \leq$ 500 MHz using a dispersion of these nanowires in saline solution at pH = 4 and 7.4 (Figures 3a and S12). This dispersion was stable throughout the measurement without the addition of any surfactant or thickener to avoid interference. Study of the relaxivity as a function of magnetic field at 25 °C clearly showed an increase at intermediate magnetic fields, reaching a maximum r_1 = 15 mM^{-1}·s^{-1} at ~40 MHz, which is more than 3 times higher than the reported relaxivity for $[GdDOTP]^{5-}$ at pH = 7.4.[22] This behavior is characteristic of slow rotational motion, typically observed in nanostructured systems.[23,24] It is important to note that, even at very high field such as 500 MHz, the relaxivity is still >6 mM^{-1}·s^{-1} at 37 °C. In addition, relaxivity increased with temperature, which indicates that the mean proton exchange between the nanowires and the bulk water is limiting relaxivity, as previously observed in other

Figure 3. (a) NMRD profile of a colloidal suspension of **nanoCAMOF-1** at pH = 4 at 25 °C (blue dot), 37 °C (red square), and 50 °C (green rhombus). (b) pH dependence of the relaxivity of **nanoCAMOF-1** measured at 40 MHz (25 °C). Error bars represent standard deviation of three replicates.

nanostructured Gd(III)-based CAs.[25] It should be mentioned that we can only obtain information on the "average" value of the proton (or water) exchange rate, as different "sites", likely having different exchange rates, can be found in this MOF. For example, Gd(III) in the porous channels and Gd(III) at the surface of the MOF will behave differently. The crystal structure shows that each Gd(III) ion inside the MOF is coordinated by six phosphonate oxygens, which yields a highly unsaturated coordination sphere for the lanthanide (typical CN = 8 or 9, at least in solution). However, it is impossible to assess the average number of water molecules per Gd(III) that contribute to the relaxivity, their distance from the paramagnetic center, and their exchange rate with bulk water. These parameters all influence the experimental relaxivity, but they cannot be assessed individually by relaxometry. The relaxivity profiles nevertheless unambiguously prove that an inner-sphere type of mechanism based on proton (or water) exchange is the major contributor to the relaxation effect in the case of **nanoCAMOF-1**. This is in contrast to other Gd(III)-containing MOFs, where only an outer-sphere contribution was operating, which yielded very low relaxivities (~1 mM^{-1}·s^{-1} at 500 MHz, 298 K).[15] The temperature dependence of the proton relaxivities allows us to draw further conclusions with respect to the mechanism. Previous reports stated that only Gd(III) centers at or near the surface are responsible for the relaxation effect,[13a,15] and those inside do not contribute. Surface Gd(III) ions have an increased hydration number; therefore, they are expected to have a fast water exchange rate.[26] The Gd(III) centers inside might have slower water exchange, or the diffusion of the water molecules through the MOF channels might be limited. The temperature increase will result in an increase of the water (or proton) exchange rate, yielding higher relaxivities.[27] The observation that the relaxivities of **nanoCAMOF-1** increase with increasing temperature therefore provides clear evidence that Gd(III) centers inside the nanoMOF do have a relaxivity contribution.

The pH dependence of the relaxivity of **nanoCAMOF-1** at 40 MHz is shown in Figure 3b. The relaxivity remains relatively

constant between pH = 4 and 9, further supporting the structural integrity of **nanoCAMOF-1** over this pH range. The small variation might be related to the protonation of surface DOTP phosphonates. This high stability motivated us to investigate the relaxivity of **nanoCAMOF-1** under physiologically more relevant conditions. To do this, the relaxivity of a dispersion of **nanoCAMOF-1** in DMEM was measured at 40 MHz over time. No significant change of the initial r_1 relaxivity of 13.05 mM^{-1}·s^{-1} was observed, even after 24 h (Figure S13). This confirms the stability of **nanoCAMOF-1** under such buffered conditions, with degradation below 10% after 24 h, as confirmed by ICP-OES.

In conclusion, we have reported the use of DOTP, a chelating ligand typically used to generate stable mononuclear lanthanide complexes, to synthesize a bimetallic Cu(II)- and Gd(III)-based MOF with promising relaxometric properties. This MOF is miniaturizable down to the nanometer length scale to form stable colloids; it is stable in water, physiological saline solution, and cell culture media; and it does not show cytotoxicity. It shows a maximum in r_1 relaxivity of 15 mM^{-1}·s^{-1} at 40 MHz, which remains constant over a wide pH range and increases with temperature. Importantly, this is the first study of the dependence of the r_1 relaxivity of a MOF as a function of a wide range of temperatures, magnetic fields, and pHs, which allowed us to conclude that an inner-sphere type of mechanism is operating and that Gd(III) centers inside the MOF structure also contribute to the relaxation effect. Synthesizing highly stable MOFs and combining their relaxometric properties and porosities should be feasible, making it possible to also exploit them in theranostics.

ASSOCIATED CONTENT

Ⓢ Supporting Information

Experimental details and additional characterization. This material is available free of charge via the Internet at http://pubs.acs.org. Further details on the crystal structure resolution may be obtained from the Cambridge Crystallographic Data Centre, on quoting the depository number CCDC-951712.

AUTHOR INFORMATION

Corresponding Authors
eva.jakabtoth@cnrs-orleans.fr
daniel.maspoch@icn.cat

Notes
The authors declare no competing financial interest.

ACKNOWLEDGMENTS

REFERENCES

(1) Merbach, A. E.; Helm, L.; Tóth, E. *The Chemistry of Contrast Agents in Medical Magnetic Resonance Imaging*, 2nd ed.; John Wiley and Sons: Chichester, 2013.

(2) (a) Aime, S.; Botta, M.; Terreno, E. *Adv. Inorg. Chem.* **2005**, *57*, 173. (b) Caravan, P.; Ellison, J. J.; McMurry, T. J.; Lauffer, R. B. *Chem. Rev.* **1999**, *99*, 2293.

(3) (a) Botta, M.; Tei, L. *Eur. J. Inorg. Chem.* **2012**, *12*, 1945. (b) Terreno, E.; Castelli, D. D.; Viale, A.; Aime, S. *Chem. Rev.* **2010**, *110*, 3019.

(4) Bridot, J.-L.; Faure, A.-C.; Laurent, S.; Rivière, C.; Billotey, C.; Hiba, B.; Janier, M.; Josserand, V.; Coll, J.-L.; Vander Elst, L.; Muller, R.; Roux, S.; Perriat, P.; Tillement, O. *J. Am. Chem. Soc.* **2007**, *129*, 5076.

(5) (a) Song, Y.; Xu, X.; MacRenaris, K. W.; Zhang, X.-Q.; Mirkin, C. A.; Meade, T. J. *Angew. Chem., Int. Ed.* **2009**, *48*, 9143. (b) Decuzzi, P.; et al. *Nat. Nanotechnol.* **2010**, *5*, 815.

(6) (a) Floyd, W. C.; Klemm, P. J.; Smiles, D. E.; Kohlgruber, A. C.; Pierre, V. C.; Mynar, J. L.; Fréchet, J. M. J.; Raymond, K. N. *J. Am. Chem. Soc.* **2011**, *133*, 2390. (b) Klemm, P. J.; Floyd, W. C.; Andolina, C. M.; Fréchet, J. M. J.; Raymond, K. N. *Eur. J. Inorg. Chem.* **2012**, *12*, 2108.

(7) Ankon, D.; Hooker, J. M.; Botta, M.; Matthew, B. F.; Aime, S.; Raymond, K. N. *J. Am. Chem. Soc.* **2008**, *130*, 2546.

(8) (a) Daldrup-Link, H. E.; Brasch, R. C. *Eur. Radiol.* **2003**, *13*, 354. (b) Liepold, L. O.; Abedin, M. J.; Buckhouse, E. D.; Frank, J. A.; Young, M. J.; Doublas, T. *Nano Lett.* **2009**, *9*, 4520.

(9) (a) Taylor, K. M. L.; Jason, S. K.; William, J. R.; Hongyu, A.; Weili, L.; Lin, W. *J. Am. Chem. Soc.* **2008**, *130*, 2154. (b) Guillet-Nicolas, R.; Bridot, J.-C.; Seo, Y.; Fortin, M.-A.; Kleitz, F. *Adv. Funct. Mater.* **2011**, *21*, 4653. (c) Tse, N. M. K.; Kennedy, D. F.; Kirby, N.; Moffat, B. A.; Muir, B. W.; Caruso, R. A.; Drummond, C. J. *Adv. Healthcare Mater.* **2013**, *2*, 836.

(10) (a) Moghaddam, M. J.; Campo, L.; Waddington, L. J.; Weerawardena, A.; Kirby, N.; Drummond, C. J. *Soft Matter.* **2011**, *7*, 10994. (b) Mulet, X.; Boyd, B. J.; Drummond, C. J. *J. Colloid Interface Sci.* **2013**, *393*, 1.

(11) Csajbók, E.; Banyai, I.; Elst, L. V.; Muller, R. N.; Zhou, W.; Petrs, J. A. *Chem.—Eur. J.* **2005**, *11*, 4799.

(12) (a) Carné, A.; Carbonell, C.; Imaz, I.; Maspoch, D. *Chem. Soc. Rev.* **2011**, *40*, 291. (b) Lin, W.; Rieter, W. J.; Taylor, K. M. L. *Angew. Chem., Int. Ed.* **2009**, *48*, 650.

(13) (a) Rieter, W. J.; Taylor, K. M. L.; An, H.; Lin, W.; Lin, W. *J. Am. Chem. Soc.* **2006**, *128*, 9024. (b) Horcajada, P.; Gref, R.; Baati, T.; Allan, P. K.; Maurin, G.; Couvreur, P.; Férey, G.; Morris, R. E.; Serre, C. *Chem. Rev.* **2012**, *112*, 1232.

(14) Taylor, K. M. L.; Jin, A.; Lin, W. *Angew. Chem., Int. Ed.* **2008**, *120*, 7836.

(15) Pereira, G. A.; Peters, J. A.; Almeida Paz, F. A.; Rocha, J.; Geraldes, C. F. G. C. *Inorg. Chem.* **2010**, *49*, 2969.

(16) Aime, S.; Botta, M.; Terreno, E.; Anelli, P. L.; Uggeri, F. *MRM* **1993**, *30*, 583.

(17) (a) Gagnon, K. J.; Perry, H. P.; Clearfield, A. *Chem. Rev* **2012**, *112*, 1034. (b) Kong, D.; Medvedev, D. G.; Clearfield, A. *Inorg. Chem.* **2004**, *43*, 7308.

(18) Sherry, A. D.; Huskens, J. R.; Brucher, E.; Tóth, E.; Geraldes, F. G. C.; Castro, M. M. C. A.; Cacheris, W. P. *Inorg. Chem.* **1996**, *35*, 4604.

(19) Geraldes, F. G. C.; Marques, M. P.; Castro, B. de; Pereira, E. *Eur. J. Inorg. Chem.* **2000**, *20*, 559.

(20) Spek, A. L. *PLATON, a Multipurpose Crystallographic Tool*; Utrecht University: Utrecht, 1998.

(21) Barge, A.; Cravotto, G.; Gianolio, E.; Fedeli, F. *Contrast Media Mol. Imaging* **2006**, *1*, 184.

(22) Laurent, S.; Vander Elst, L.; Muller, R. N. *Contrast Media Mol. Imaging* **2006**, *1*, 128.

(23) Tsotsalas, M.; Busby, M.; Gianolio, E.; Aime, S.; De Cola, L. *Chem. Mater.* **2008**, *20*, 5888.

(24) Guari, Y.; Larionova, J.; Corti, M.; Lascialfari, A.; Marinone, M.; Poletti, G.; Molvinger, K.; Guérien, C. *Dalton Trans.* **2008**, 3658.

(25) Platas-Iglesias, C.; Elst, L. V.; Zhou, W.; Muller, R. N.; Geraldes, F. G. C.; Maschmeyer, T.; Peters, J. A. *Chem.—Eur. J.* **2002**, *8*, 5124.

(26) Helm, L.; Merbach, A. E. *Chem. Rev.* **2005**, *105*, 1923.

(27) Merbach, A. E.; Helm, L.; Tóth, E. *The Chemistry of Contrast Agents in Medical Magnetic Resonance Imaging*, 2nd ed.; John Wiley and Sons: Chichester, 2013; Chapter 2.